

## Heterocycles | Hot Paper |

 Triptycene End-Capped Benzothienobenzothiophene and NaphthothienobenzothiopheneLucas Ueberricke,<sup>[a]</sup> Julia Schwarz,<sup>[a]</sup> Farhad Ghalami,<sup>[b]</sup> Maik Matthiesen,<sup>[c]</sup> Frank Rominger,<sup>[a]</sup> Sven M. Elbert,<sup>[a]</sup> Jana Zaumseil,<sup>[c]</sup> Marcus Elstner,<sup>[b]</sup> and Michael Mastalerz<sup>\*[a]</sup>

**Abstract:** Previously it was demonstrated that triptycene end-capping can be used as a crystal engineering strategy to direct the packing of quinoxalinophenanthrophenazines (QPPs) towards cofacially stacked  $\pi$  dimers with large molecular overlap resulting in high charge transfer integrals. Remarkably, this packing motif was formed under different crystallization conditions and with a variety of derivatives bearing additional functional groups or aromatic substitu-

ents. Benzothienobenzothiophene (BTBT) and its derivatives are known as some of the best performing compounds for organic field-effect transistors. Here, the triptycene end-capping concept is introduced to this class of compounds and polymorphic crystal structures are investigated to evaluate the potential of triptycene end-caps as synthons for crystal engineering.

## Introduction

Many properties of molecular materials, like for example charge transport in organic semiconductors, strongly depend on the relative arrangement of the molecules in the solid state and finding the right packing is often a challenging task.<sup>[1]</sup> In the field of crystal engineering there are a few structural motifs of high directionality, such as hydrogen<sup>[2]</sup> or halogen bonding,<sup>[3]</sup> that efficiently allow to control the molecular packing. Other supramolecular interactions, such as  $\pi$  stacking are much less directional.<sup>[4]</sup> This is unfortunate, as it is the relative orientation of the  $\pi$  planes that has a significant impact on charge transport, which is essential for efficiently working organic electronic devices, like organic field-effect transistors (OFETs).<sup>[5]</sup> Since a few years, we have been studying the effect of triptycene end-capping of larger annulated aromatic compounds on their solubility and packing in the solid state.


Whereas two triptycene end-caps significantly increases the solubility,<sup>[6]</sup> one triptycene end-cap is functioning as a directing unit to foster the  $\pi$ -planes to stack in a nearly eclipsed fashion with high “overlap” of the frontier molecular orbitals.<sup>[6d]</sup> Based on these findings a number of one-fold triptycene end-capped quinoxalinophenanthrophenazines (QPPs) were synthesized and the impact of various functional groups on packing of the QPPs studied. To our delight, almost independently from the substitution patterns we found for nearly all QPPs the same type of cofacial  $\pi$  stacking with large molecular overlap,<sup>[7]</sup> suggesting that the triptycene end-capping strategy can be used as kind of a crystal-engineering synthon to arrange larger  $\pi$ -systems in an advantageous fashion. For some of the QPP crystals high charge transfer integrals of up to 190 meV were calculated, demonstrating that these structures are potential candidates for OFET devices.<sup>[7a]</sup>


One of the most efficient *p*-type semiconductors is benzothienobenzothiophene (BTBT) and derivatives thereof.<sup>[8]</sup> Due to its electronic structure with a low-lying highest occupied molecular orbital (HOMO) it combines high hole mobility with a good air stability.<sup>[9]</sup> Several derivatives of BTBT bearing additional substituents, such as alkyl chains<sup>[8b]</sup> or aromatic substituents,<sup>[8a]</sup> as well as BTBT dimers<sup>[8c]</sup> and derivatives with an extended  $\pi$  plane<sup>[8e–h, 10]</sup> have already been successfully used in OFET devices. Using BTBT decorated with octyl chains for spin-coated OFETs, maximum mobilities of up to  $43 \text{ cm}^2 \text{ V}^{-1} \text{ s}^{-1}$  were reported.<sup>[10]</sup> In these derivatives, like in the parent BTBT, the aromatic planes usually arrange in a herringbone motif with transfer integrals of 58 meV for the parent BTBT for edge-to-face-stacked molecules and up to 91 meV for the corresponding dinaphtho derivative. SC-OFET devices with the latter showed high performance with hole mobilities up to  $8.3 \text{ cm}^2 \text{ V}^{-1} \text{ s}^{-1}$ .<sup>[8b,c,f–h, 9a, 11]</sup> Only for derivatives with larger  $\pi$  planes face-to-face molecular overlap could be realized, how-

[a] L. Ueberricke, J. Schwarz, Dr. F. Rominger, Dr. S. M. Elbert, Prof. Dr. M. Mastalerz  
Organisch-Chemisches Institut, Ruprecht-Karls-Universität Heidelberg  
Im Neuenheimer Feld 270, 69120 Heidelberg (Germany)  
E-mail: Michael.mastalerz@oci.uni-heidelberg.de

[b] F. Ghalami, Prof. Dr. M. Elstner  
Institut für Physikalische Chemie, Karlsruher Institute of Technology (KIT)  
Kaiserstr. 12, 76131 Karlsruhe (Germany)

[c] M. Matthiesen, Prof. Dr. J. Zaumseil  
Institut für Physikalische Chemie, Universität Heidelberg  
Im Neuenheimer Feld 253, 69120 Heidelberg (Germany)

 Supporting information and the ORCID identification number(s) for the author(s) of this article can be found under:  
<https://doi.org/10.1002/chem.202001125>.

 © 2020 The Authors. Published by Wiley-VCH GmbH. This is an open access article under the terms of Creative Commons Attribution NonCommercial-NoDerivs License, which permits use and distribution in any medium, provided the original work is properly cited, the use is non-commercial and no modifications or adaptations are made.

ever along the  $\pi$  stacking axis a small transfer integral of 12 meV was calculated. Consequently, a modest mobility ( $0.14 \text{ cm}^2 \text{ V}^{-1} \text{ s}^{-1}$ ) was measured.<sup>[8e]</sup>

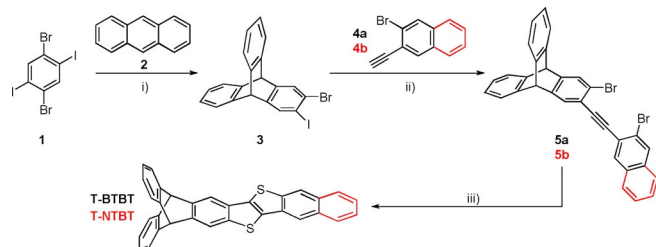
We envisioned that triptycene end-capping of BTBT and congeners thereof possibly also has a directing effect towards more favorable stacking motifs with increased  $\pi$  stacking and thus higher transfer integrals, which in principle can further enhance the charge transport properties of BTBTs. Here, we present the synthesis and crystallographic studies of triptycene substituted BTBT derivatives as well as their potential ability for charge transfer.

## Results and Discussion

### Synthesis and characterization

Both target molecules were accessible through a three-step synthesis (Scheme 1). Commercially available dibromodiiodo benzene **1** was treated with one equivalent of *n*BuLi to generate the corresponding aryl anion in situ, which subsequently reacts with anthracene **2** in a Diels–Alder reaction to give bromiodo triptycene **3** in 16% yield. Sonogashira–Hagihara cross-coupling of **3** with alkynes **4a** and **4b** gave compounds **5a** and **5b** in 83 and 84% yields, respectively. All products were characterized by  $^1\text{H}$  and  $^{13}\text{C}$  NMR spectroscopy, IR spectroscopy, mass spectrometry and elemental analysis. The structures of bromiodo triptycene **3** and alkyne **5a** could additionally be confirmed by single-crystal X-ray diffraction (see Supporting Information for details).

Final step is a copper catalyzed cyclisation with sodium sulfide<sup>[12]</sup> giving triptycene end-capped benzothienobenzothiophene (T-BTBT) and naphthothienobenzothiophene (T-NTBT). T-BTBT was isolated in 50% yield after recrystallization from acetone and could be further purified by sublimation ( $270^\circ\text{C}$ ,  $3 \times 10^{-3}$  mbar) in a Kugelrohr oven. For T-NTBT the purification was more tedious. After column chromatography followed by recrystallization from petroleum ether/ $\text{CHCl}_3$  only 6% could be isolated. Both target compounds were characterized by  $^1\text{H}$  and  $^{13}\text{C}$  NMR spectroscopy, IR spectroscopy, HR mass spectrometry (DART) and elemental analysis as well as single-crystal X-ray diffraction (see below). In the  $^1\text{H}$  NMR spectrum of T-BTBT two singlets at  $\delta = 7.90$  ppm and 7.89 ppm were found for the two inner phenylene protons  $H^b$  and  $H^{b'}$  of the triptycene end-cap (Figure 1, top).



**Scheme 1.** Synthesis of T-BTBT and T-NTBT. Conditions: i) *n*BuLi (1.60 equiv), toluene (abs.), Ar, 17 h, rt, 16%. ii) 5 mol%  $\text{Pd}(\text{PPh}_3)_2\text{Cl}_2$ , 10 mol% CuI,  $\text{NEt}_3$ , THF, Ar, 14 h, rt, 83% (**5a**), 84% (**5b**); iii)  $\text{Na}_2\text{S}\cdot x\text{H}_2\text{O}$  (4.00 equiv),  $\text{I}_2$  (2.00 equiv), CuI (0.20 equiv), NMP, Ar, 24 h,  $120^\circ\text{C}$ , 50% (T-BTBT), 6% (T-NTBT).

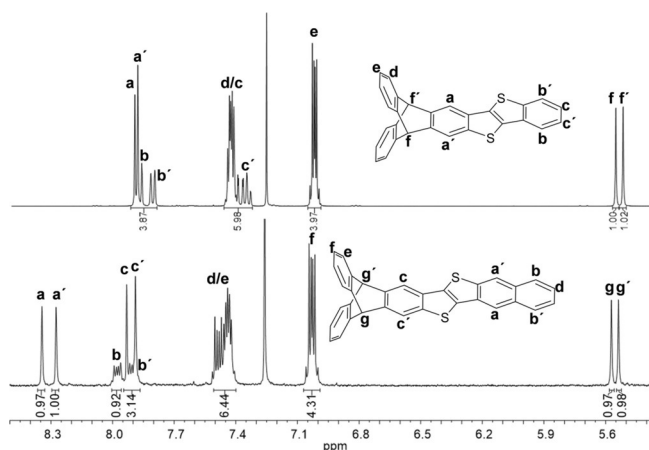


**Figure 1.**  $^1\text{H}$  NMR spectra (400 MHz,  $\text{CDCl}_3$ ) of T-BTBT (top) and T-NTBT (bottom).

The protons of the peripheral phenylene units of the triptycene end-cap  $H^b$  and  $H^{b'}$  resonate as doublet of doublets at  $\delta = 7.88$  ppm, 7.81 ppm and as doublet of triplets at  $\delta = 7.36$  ppm. The signals of  $H^b$  and  $H^{b'}$  overlap with the signal of the protons  $H^d$  and  $H^e$ . The characteristic bridgehead protons of the triptycene  $H^f$  and  $H^f'$  can be found at  $\delta = 5.56$  ppm and  $\delta = 5.52$  ppm, while the multiplet at  $\delta = 7.45$ –7.42 ppm and the doublet of doublets at  $\delta = 7.03$  ppm can be assigned to the protons of the unsubstituted triptycene wings  $H^d$  and  $H^e$ . The  $^1\text{H}$  NMR spectrum of T-NTBT shows signals with similar chemical shifts and multiplicity. The two additional protons of the naphthalene unit  $H^g$  and  $H^{g'}$  can be found as two singlets at  $\delta = 8.34$  ppm and  $\delta = 8.27$  ppm (Figure 1, bottom).

### Optoelectronic properties

T-BTBT and T-NTBT have been investigated by UV/Vis and fluorescence spectroscopy in dichloromethane (Figure 2 and Table 1). T-BTBT shows a similar absorption spectrum as the

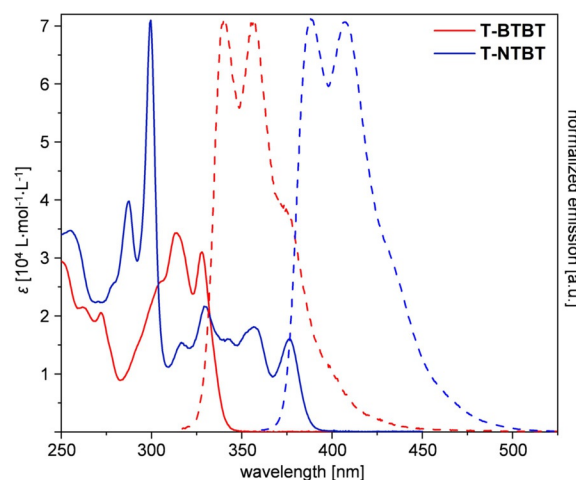


**Figure 2.** Absorption (bold line) and emission spectra (dotted line) of T-BTBT and T-NTBT, measured in  $\text{CH}_2\text{Cl}_2$  ( $2 \mu\text{M}$ ) at rt.

Table 1. Optoelectronic and electrochemical properties of T-BTBT and T-NTBT.											
Compound	$\lambda_{\text{abs}}^{[a,b]}$ [nm]	$\lambda_{\text{onset}}$ [nm]	$\lambda_{\text{em}}^{[a]}$ ( $\lambda_{\text{ex}}$ ) [nm]	$E_{\text{Stokes}}$ [cm <sup>-1</sup> ]	$\Phi^{[a]}$ [%]	$E_{\text{g(opt)}}^{[c]}$ [eV]	$E^{\text{ox}[d]}$ [V]	$E_{\text{HOMO}}^{\text{DFT}[e]}$ [eV]	$E_{\text{LUMO}}^{\text{DFT}[e]}$ [eV]	$E_{\text{g}}^{\text{DFT}[e]}$ [eV]	$\lambda^+[f]$ [meV]
T-BTBT	328	339	340 357 373 (318)	1076	15	3.7	0.94	-5.8	-1.6	4.2	188
T-NTBT	375	388	388 406 428 <sup>sh</sup> (365)	894	18	3.2	0.82	-5.5	-1.9	3.6	155

[a] Measured in CH<sub>2</sub>Cl<sub>2</sub> at rt. [b] Absorption maximum at the longest wavelength. [c] Estimated from onset;  $E_{\text{g(opt)}} = 1242/\lambda$ . [d] Cyclic voltammogram obtained in CH<sub>2</sub>Cl<sub>2</sub> with a Pt electrode and nBu<sub>4</sub>NPF<sub>6</sub> as the electrolyte. Scan speed: 50 mV s<sup>-1</sup>; ferrocene/ferrocenium (Fc/Fc<sup>+</sup>) was used as internal reference. [e] obtained from quantum-chemical calculations using DFT-B3LYP/6-311++G\*\*. [f] reorganization energy calculated by DFT-B3LYP/6-31G\*. sh: shoulder.

parent BTBT ( $\lambda_{\text{max}} = 332$  nm).<sup>[9b]</sup> The absorption peaks at  $\lambda_{\text{abs}} = 328$  and 314 nm correspond to the  $p$ -bands, while absorption maxima at  $\lambda_{\text{abs}} = 272$  and 262 nm can be assigned to the  $\beta$ -bands in agreement with the isoelectronic structure of chrysenes.<sup>[9,13]</sup> Emission maxima can be found at  $\lambda_{\text{em}} = 340, 357$  and 373 nm. This corresponds to a Stokes shift of  $E_{\text{Stokes}} = 1076$  cm<sup>-1</sup>. From  $\lambda_{\text{onset}} = 339$  nm an optical band gap of  $E_{\text{g,opt}} = 3.7$  eV was estimated. The absorption bands of T-NTBT are bathochromically shifted compared to T-BTBT with absorption peaks at  $\lambda_{\text{abs}} = 375, 356, 329, 316, 299, 287$  and 255 nm and are similar to the parent NTBT system ( $\lambda_{\text{max}} = 376$  nm).<sup>[8g]</sup> The molar extinction coefficient of the peaks  $\lambda_{\text{abs}} = 299$  and 287 nm are greatly enhanced compared to T-BTBT. Emission maxima are found at  $\lambda_{\text{em}} = 388$  and 406 nm with an additional shoulder at 428 nm, resulting in a slightly lower Stokes shift of  $E_{\text{Stokes}} = 894$  cm<sup>-1</sup> compared to T-BTBT, indicating smaller reorganization energy for the transition of the ground state to the first excited state. The optical bandgap estimated from the absorption onset ( $\lambda_{\text{onset}} = 388$  nm) is  $E_{\text{g,opt}} = 3.2$  eV. The photoluminescent quantum yields for both T-BTBT and T-NTBT in CH<sub>2</sub>Cl<sub>2</sub> solution are within a narrow range of 15 and 18%, respectively.

By cyclic voltammetry (CV) in dichloromethane T-BTBT showed a quasi-reversible oxidation potential at  $E^{\text{ox}} = 0.94$  V, which is slightly lower than the potential reported for the parent BTBT (1.02 V).<sup>[14]</sup> For T-NTBT the oxidation potential was lower ( $E^{\text{ox}} = 0.82$  V) (Figure 3).

For both compounds DFT calculations (B3LYP: 6-311++G\*\*) were performed (Figure 4 and Table 1). They show that for both T-BTBT and T-NTBT the HOMO and LUMO orbitals are delocalized over the whole BTBT, respectively NTBT backbone. For T-BTBT the calculated HOMO and LUMO levels are  $E_{\text{HOMO}}^{\text{DFT}} = -5.8$  eV and  $E_{\text{LUMO}}^{\text{DFT}} = -1.6$  eV. A slightly lower LUMO level ( $E_{\text{LUMO}}^{\text{DFT}} = -1.9$  eV) and slightly higher HOMO level ( $E_{\text{HOMO}}^{\text{DFT}} = -5.5$  eV) was calculated for T-NTBT, resulting in a smaller band gap ( $E_{\text{g}} = 3.6$  eV) compared to T-BTBT ( $E_{\text{g}} = 4.2$  eV).

Reorganization energies for hole transport  $\lambda^+$ ,<sup>[15]</sup> which describe the strength of local electron-phonon coupling, strongly affect the charge transport properties.<sup>[16]</sup> For high carrier mobilities small reorganization energies are desired.<sup>[17]</sup> DFT calculations (B3LYP 6-31G\*) revealed a reorganization energy for hole

transport of  $\lambda^+ = 188$  meV for T-BTBT and  $\lambda^+ = 155$  meV for T-NTBT.<sup>[9a]</sup> Both values are comparable to related thiophene based compounds<sup>[9a,16a]</sup> or rubrene (159 meV),<sup>[118]</sup> but substantial larger than the reorganization energy of pentacene

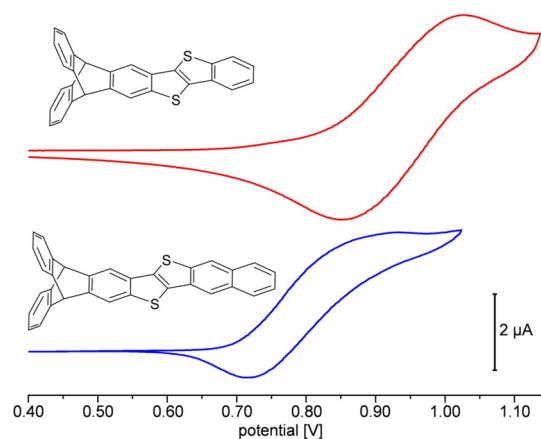


Figure 3. Cyclic voltammograms of T-BTBT and T-NTBT (CH<sub>2</sub>Cl<sub>2</sub>, nBu<sub>4</sub>NPF<sub>6</sub> (0.1 M), measured at room temperature with a Pt electrode and Fc/Fc<sup>+</sup> as internal reference (scanning speed: 50 mV s<sup>-1</sup>).

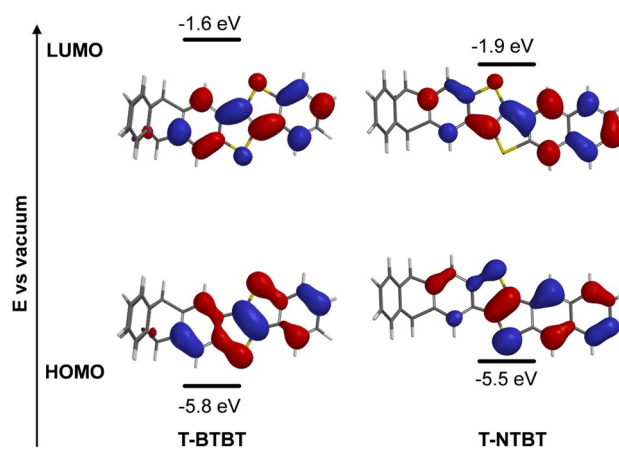


Figure 4. HOMO-LUMO diagram of T-BTBT and T-NTBT (calculated using DFT-B3LYP: 6-311++G\*\*).

(97 meV).<sup>[19]</sup> Notably, the parent BTBT has a significantly larger reorganization energy (226 meV)<sup>[14]</sup> than **T-BTBT**, suggesting that the triptycene end-capping positively affects this parameter. This may be explained by homoconjugation of the unsubstituted triptycene wings,<sup>[20]</sup> which effectively increases the delocalization of the hole in the radical-cation state, thereby reducing structural deformation during the carrier transport.

### Single-crystal X-ray structure analysis

As already mentioned in the introduction, we were interested in how the triptycenylenyl unit affects the packing in the crystalline state and if it has a similar effect than prior observed for the QPP systems.<sup>[7a,b]</sup> **T-BTBT** showed a high crystallization tendency and five different crystal structures were obtained. The first crystal (solvate  $\alpha$ ) was grown by vapor diffusion of ethanol into a chloroform solution. It crystallized in the orthorhombic space group  $P2_12_12_1$  with eight molecules in the unit cell and two **T-BTBT** molecules and one chloroform molecule in the asymmetric unit (Figure 5a). The two **T-BTBT** molecules are arranged in an edge-to-face orientation and interact via short C...S contacts<sup>[8c]</sup> between a sulfur atom and one of the central carbon atoms of the BTBT backbone ( $A_{CS}$ ,  $d_{C...S}=3.35$  Å). **T-BTBT** molecules assemble in a herringbone fashion (Figure 5b) with infinite edge-to-face stacked sheets ( $D_{SS/H}$ ) along the crystallographic  $b$  axis, in which the molecules additionally interact via S...H<sup>[8c]</sup> ( $d_{S...H}=2.94$  Å) and S...S contacts<sup>[21]</sup> ( $d_{S...S}=3.64$  Å) (Figure 5e). Molecules of adjacent herringbone sheets form antiparallel face-to-face  $\pi$  stacked dimers ( $C_{||}$ ) with  $d_{\pi... \pi}=3.47$  Å (Figure 5c and d) in the same fashion as previously observed for the QPPs,<sup>[7a]</sup> indicating that the postulated directing effect of the triptycenylenyl end-capping<sup>[7a]</sup> can be observed also for this system, albeit to a lesser degree. Edge-to-face  $\pi$ -stacked dimers ( $B_{\perp}$ ) also exist with  $d_{C...H}=2.77$  Å. Chloroform molecules are located in the voids formed by the unsubstituted triptycene wings. Other crystallization conditions have also been tested. When crystallized by slow evaporation of an acetone solution, a very similar structure was obtained (solvate  $\beta$ , see Figure S45 a–d). Again, **T-BTBT** crystallized in the orthorhombic space group  $P2_12_12_1$  with eight molecules in the unit cell and two **T-BTBT** molecules and one acetone molecule in the asymmetric unit. The packing is isostructural to the  $\alpha$  sol-

vate with only small differences in relative orientation of the molecules and a slightly larger cell volume.

Upon vapor diffusion of ethanol into a toluene solution, **T-BTBT** crystallized in the orthorhombic space group  $Pca2_1$  with eight molecules in the unit cell and two molecules in the asymmetric unit (polymorph  $\gamma$ ). The packing is very similar to solvates  $\alpha$  and  $\beta$  (see above), but without enclathrated solvent molecules. Here too, a herringbone pattern is formed with infinite sheets of edge-to-face  $\pi$  stacked molecules along the crystallographic  $c$  axis with additional S...S interactions ( $d_{S...S}=3.60$  Å). Additionally, antiparallel face-to-face stacked dimers with  $d_{\pi... \pi}=3.45$  Å between adjacent sheets are observed (see Figure S45 e–i). The fourth modification was obtained by sublimation in a Kugelrohr oven at 270 °C under vacuum ( $3 \times 10^{-3}$  mbar). Under these conditions **T-BTBT** crystallized in the orthorhombic space group  $Pca2_1$  with four molecules per unit cell and one molecule in the asymmetric unit (Figure 6; polymorph  $\delta_1$ ). The molecules packed in a rather unexpected manner. The overall packing can be visualized as a herringbone-type motif with increased face-to-face  $\pi$  interactions along the crystallographic  $a$  axis (Figure 6a). In contrast to the previously described structures, adjacent **T-BTBT** molecules are interacting via the thiophene units in a cross-shaped fashion (Figure 6b), forming one-dimensional face-to-face stacked columns with a short distance of the  $\pi$ -systems ( $A_{||}$ ,  $d_{\pi... \pi}=3.42$  Å) (Figure 6c). Within these columns edge-to-face  $\pi$  stacking ( $d_{CH... \pi}=2.88$  Å) between the unsubstituted triptycenylenyl wing and the BTBT backbone as well as C...S interactions ( $d_{C...S}=3.49$ – $3.51$  Å) stabilize the structure. Adjacent columns interact via weak van-der-Waals interactions ( $B_{vdW}$ ,  $d_{C...H}=2.85$  Å). Along the  $\pi$  stacking axis the structure is stabilized by edge-to-face  $\pi$  stacking ( $d_{\pi... \pi, \perp}=2.88$  Å) between the unsubstituted triptycene wing and the BTBT backbone of adjacent molecules (Figure 6c). Single crystals were also grown by sublimation using a constant argon flow through a horizontal tube, on which a temperature gradient was applied. The bulk material was placed in the hottest zone at 280 °C. In the colder zones crystals of different morphology re-sublimated within the same batch. For a plate-like crystal the same unit cell as found in polymorph  $\delta_1$  was determined. On the other hand, different bulky polyedric crystals were obtained. Here, **T-BTBT** crystallized in the monoclinic space group  $C2/c$  with eight molecules

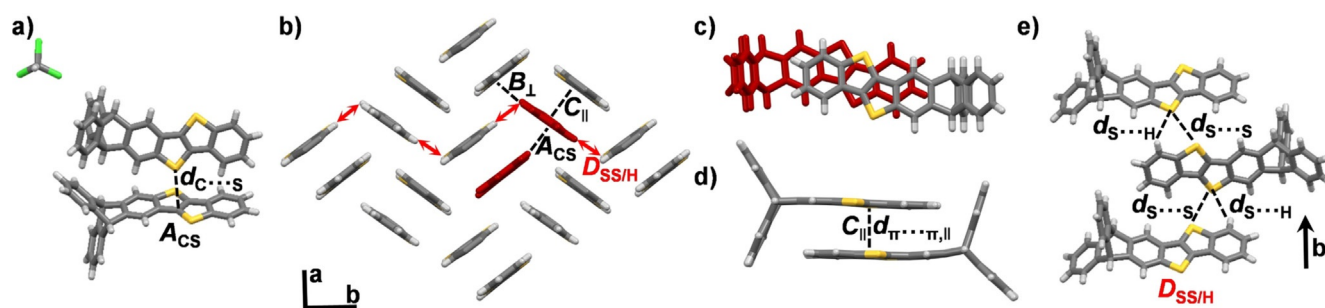


**Figure 5.** Single-crystal X-ray structure of **T-BTBT** (solvate  $\alpha$ ) crystallized by vapor diffusion of EtOH into a  $\text{CHCl}_3$  solution: a) Asymmetric unit. b) Herringbone packing (triptycene end-caps omitted for clarity); asymmetric unit colored in red (solvent molecules omitted for clarity). Infinite edge-to-face stacking pattern along the crystallographic  $b$  axis indicated with red arrows. c, d) Antiparallel face-to-face stacked dimer from top (c) and side (d) view. e) S...S and S...H short contacts along the  $b$  axis.

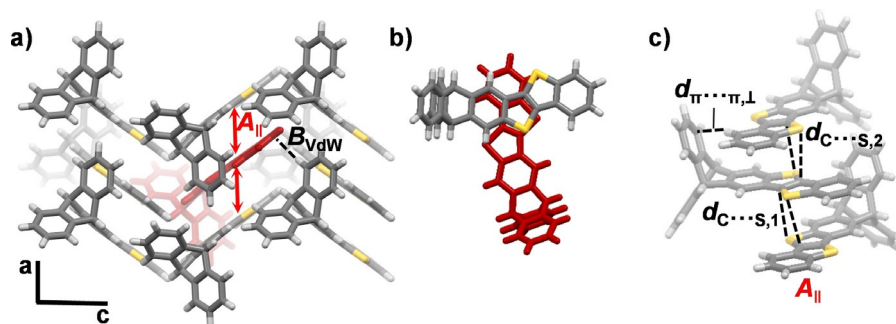


**Figure 6.** Single-crystal X-ray structure of **T-BTBT** (polymorph  $\delta_1$ ) crystallized by sublimation at the Kugelrohr oven (270 °C,  $3 \times 10^{-3}$  mbar): a) herringbone packing. Asymmetric unit colored in red. Infinite  $\pi$ -stacking patterns along the crystallographic  $a$  axis indicated by arrows. b) Structural overlap of a  $\pi$  stacked dimer. c) Short contacts within a  $\pi$  stacked column.

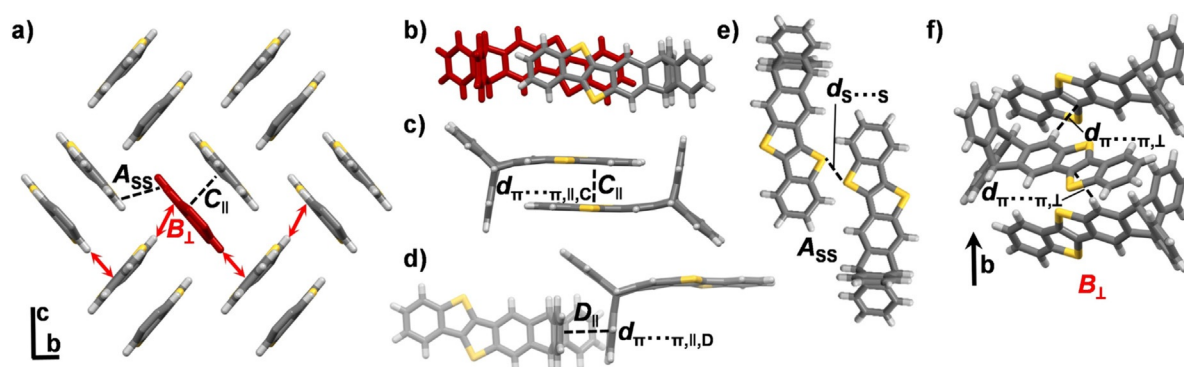


**Figure 7.** Single-crystal X-ray structure of **T-BTBT** (polymorph  $\delta_2$ ) crystallized by sublimation in an argon stream and temperature gradient (starting temperature: 280 °C): a) packing.  $\pi$ -stacking patterns indicated by arrows. b, c) Antiparallel face-to-face stacked dimer from top (b) and side (c) view. d)  $\pi$ -Stacking between adjacent triptycene end-caps. e) S...S contacts. f) Edge-to-face stacking along the  $b$  axis.

per unit cell and one molecule in the asymmetric unit (polymorph  $\delta_2$ ). Here, again a herringbone packing formed with infinite edge-to-face stacks ( $B_{\perp}$ ,  $d_{C...H} = 2.67$  Å) along the crystallographic  $b$  axis (Figure 7a and f). Adjacent herringbone sheets interact via edge-to-face stacking ( $B_{\perp}$ ,  $d_{\pi...,\pi,\perp} = 2.67$  Å) and antiparallel  $\pi$  face-to-face-stacked dimers ( $C_{\parallel}$ ,  $d_{\pi...,\pi} = 3.43$  Å) (Figure 7b & c). Although similar to the previous ones, this packing is stabilized by additional  $\pi$  stacking of adjacent unsubstituted triptycene-wings ( $d_{\pi...,\pi} = 3.72$  Å), forming a layered structure. Adjacent layers interact via S...S contacts ( $d_{S...S} = 3.61$  Å) (Figure 7e).

The polymorphism observed during sublimation by the argon stream method is only a minor drawback, as the two polymorphs can be simply distinguished by their shape (see the Supporting Information).

For **T-NTBT** single-crystals were obtained by sublimation in a Kugelrohr oven (230 °C,  $5 \times 10^{-3}$  mbar). **T-NTBT** crystallized in the triclinic space group  $P\bar{1}$  with two molecules per unit cell and one molecule in the asymmetric unit. The packing is analogous to the one of the previously reported triptycene end-capped QPPs.<sup>[7a]</sup> Two antiparallel  $\pi$  stacked dimers with different molecular overlap (Figure 8a and b) with  $d_{\pi...,\pi A} = 3.59$  Å and  $d_{\pi...,\pi B} = 3.52$  Å alternate and form a layered structure stabilized by  $\pi$  stacking of unsubstituted triptycene wings ( $d_{\pi...,\pi C} = 3.83$  Å) (8c). Adjacent layers interact via S...S contacts

( $d_{S...S} = 3.35$ – $3.56$  Å) (Figure 8d). Table 2 summarizes the crystallographic details.

### Calculated charge transfer integrals

In order to evaluate the potential of the obtained structures as OFET materials, the electronic couplings between adjacent molecules of all obtained crystal structures were calculated. The electronic coupling, between molecules can be used to quantify the charge transport capability. Based on the molecular system, the orientation between the molecules and their corresponding couplings differ, which results in varying mobilities. For example, the charge transport mobility in an anthracene crystal differs with respect to the orientation of the molecules along the crystal axes  $a$ ,  $b$  and  $c$ .<sup>[22]</sup> Therefore, HOMO transfer integrals ( $t_h$ ) responsible for hole transport were calculated using the DFTB method (Table 3; see the Supporting Information for details on the calculation).<sup>[23]</sup>

The calculations reveal that in the  $\alpha$  modification of **T-BTBT** the strongest coupling ( $t_h^{C_{\parallel}} = 33$  meV) exists between the antiparallel face-to-face  $\pi$  stacked dimers (Figure 5c and d) and is approx. as high as the coupling between two edge-to-face stacked molecules ( $t_h^{B_{\perp}} = 32$  meV). Edge-to-face stacked molecules with additional C...S and S...S contacts (Figure 5a and e) have lower transfer integrals (10–16 meV). As a continuous

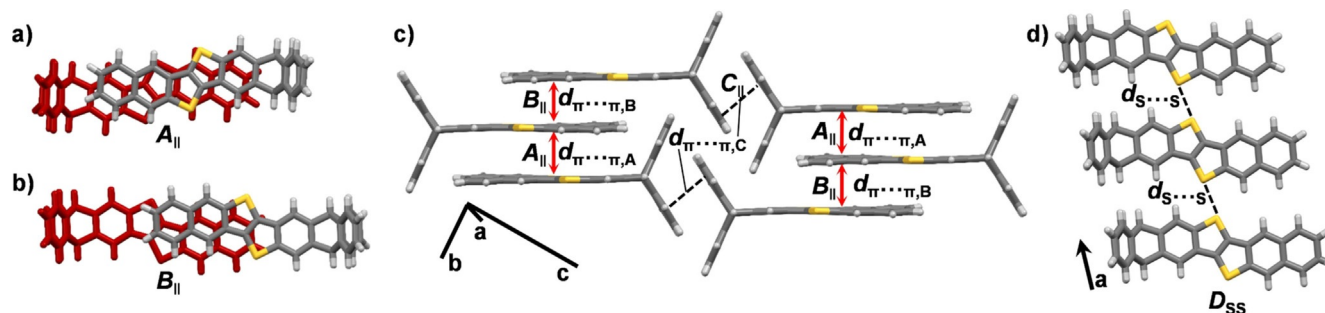


**Figure 8.** Single crystal X-ray structure of **T-NTBT** (polymorph  $\alpha$ ) crystallized by sublimation at the Kugelrohr oven (230 °C,  $5 \times 10^{-3}$  mbar): a, b) Structural overlap of two different  $\pi$  dimers. c) Packing.  $\pi$ -stacking patterns indicated by arrows. d) S...S contacts.

#	Compound	Method	Space group	$N_{\text{asym}}$ <sup>[d]</sup>	$Z$ <sup>[e]</sup>	$d_{\pi-\pi}$ [Å] <sup>[f]</sup>	Other short contacts [Å] <sup>[a]</sup>
1	<b>T-BTBT</b>	$\text{CHCl}_3/\text{EtOH}$ , <sup>[b]</sup> $\alpha$	$P2_12_12_1$ (orthorhombic)	2	8	3.47	3.35–3.42 (C...S), 3.64 (S...S), 2.94 (S...H), 2.77 (C...H)
2	<b>T-BTBT</b>	acetone, <sup>[c]</sup> $\beta$	$P2_12_12_1$ (orthorhombic)	2	8	3.45	3.31 (C...S), 3.60–3.94 (S...S), 2.92 (S...H), 2.78 (C...H)
3	<b>T-BTBT</b>	toluene/ $\text{EtOH}$ , <sup>[b]</sup> $\gamma$	$Pca2_1$ (orthorhombic)	2	8	3.45	3.26–3.47 (C...S), 3.60 (S...S), 2.82 (C...H)
4	<b>T-BTBT</b>	sublimation (vacuum); $\delta_1$	$Pca2_1$ (orthorhombic)	1	4	3.42	3.49–3.51 (C...S), 2.88 (C...H)
5	<b>T-BTBT</b>	physical vapor transport (Ar stream); $\delta_2$	$C2/c$ (monoclinic)	1	8	3.43	3.61 (S...S), 2.67–2.89 (C...H), 3.72 ( $\pi \cdots \pi$ , 2)
6	<b>T-NTBT</b>	sublimation (vacuum); $\alpha$	$P\bar{1}$ (triclinic)	1	2	3.59 (1) 3.52 (2)	3.35–3.56 (S...S), 3.83 ( $\pi \cdots \pi$ , 3)

[a] Values have been determined for two adjacent molecules. For the determination procedure, see the Supporting Information. [b] Gas diffusion of ethanol at rt. [c] Slow evaporation of solvent at rt. [d] Number of molecules in the asymmetric unit; refined solvate molecules not counted. [e] Total number of molecules in the unit cell including refined solvate molecules. [f]  $\pi$ - $\pi$  distances of the BTBT unit; the numbers in brackets indicate the  $\pi$  stacking motifs as shown in Figure 5–Figure 8;  $\pi$ -planes were calculated from all atoms of the aromatic backbone.

#	Compound	modification <sup>[a]</sup>	A <sup>[a,b]</sup>	B <sup>[a,b]</sup>	C <sup>[a,b]</sup>	D <sup>[a,b]</sup>	Preferred charge transfer direction <sup>[d]</sup>
1	<b>T-BTBT</b>	$\alpha$	10 (C...S)	32 ( $\pi \cdots \pi_{\perp}$ )	33 ( $\pi \cdots \pi_{\parallel}$ )	<b>16</b> (S...S/H)	$b$ axis
2	<b>T-BTBT</b>	$\beta$	24 ( $\pi \cdots \pi_{\parallel}$ )	20 ( $\pi \cdots \pi_{\perp}$ )	12 (C...S)	<b>18</b> (S...S/H)	$b$ axis
3	<b>T-BTBT</b>	$\gamma$	22 (C...S)	19 ( $\pi \cdots \pi_{\perp}$ )	11 ( $\pi \cdots \pi_{\parallel}$ )	<b>4</b> (S...S)	$c$ axis
4	<b>T-BTBT</b>	$\delta_1$	<b>177</b> ( $\pi \cdots \pi_{\parallel}$ )	28 (VdW)	–	–	$a$ axis
5	<b>T-BTBT</b>	$\delta_2$	92 (S...S)	<b>27</b> ( $\pi \cdots \pi_{\perp}$ )	44 ( $\pi \cdots \pi_{\parallel}$ )	0 ( $\pi \cdots \pi_{\parallel}$ ) <sup>[c]</sup>	$b$ axis
6	<b>T-NTBT</b>	$\alpha$	116 ( $\pi \cdots \pi_{\parallel}$ )	<b>71</b> ( $\pi \cdots \pi_{\parallel}$ )	0 ( $\pi \cdots \pi_{\parallel}$ ) <sup>[c]</sup>	23 (S...S)	$\pi$ stack axis

[a] See Figures 5–8 and Table 2. [b] dimers interacting via short contacts indicated in brackets. All values given in meV. [c]  $\pi$  stacked unsubstituted triptycene wings. [d] Indicated by red arrows in Figures 6–8; corresponding transfer integrals highlighted in bold.

stacking motif is required for charge transport to take place, the edge-to-face arranged molecules with S...S and S...H contacts (Figure 5b and e) most likely determine the transport properties. As they assemble along the crystallographic  $b$  axis, charge transport with a transfer integral of  $t_h^{D,SS} = 16$  meV in this direction is presumably preferred over other directions. Due to the very similar structure (see Figure S45 a–d), the couplings for the  $\beta$  solvate are in the same range with only a smaller transfer integral for the antiparallel face-to-face  $\pi$  stacked dimer ( $t_h^{A,||} = 24$  meV). For the  $\gamma$  modification (see the Supporting Information) transfer integrals are generally lower (4–22 meV), which might be explained by different relative ori-

entation of adjacent molecules. The largest coupling exists between the edge-to-face arranged dimers with C...S short contact ( $t_h^{A,CS} = 22$  meV). The preferred hole transport direction here is the herringbone sheet with continuous S...S short contacts along the crystallographic  $c$  axis (Figure S45f,i) with only poor coupling ( $t_h^{D,SS} = 4$  meV). The  $\delta_1$  polymorph continuously stacks along the crystallographic  $a$  axis (Figure 6a). With  $t_h^{A,||} = 177$  meV the coupling in this direction is exceptionally high, not only compared to the parent BTBT ( $t_h = 58$  meV),<sup>[8c]</sup> but also compared to other compounds with high hole mobilities like pentacene ( $t_h = 75$  meV),<sup>[24]</sup> hexacene ( $t_h = 88$  meV)<sup>[25]</sup> or rubrene ( $t_h = 100$  meV).<sup>[26]</sup> This makes this packing motif very

promising for potential OFET devices. In fact only a few compounds with comparably high hole transfer integrals (170–190 meV) have been reported so far.<sup>[7a,9a,16a]</sup> Noteworthy, the coupling between the cross-wise  $\pi$  stacking in  $\delta_1$  (Figure 6b) is much higher compared to the antiparallel  $\pi$  stacking found in the other modifications, despite the smaller molecular overlap. This might be attributed to an enhanced HOMO orbital overlap of the orbital lobes of the thiophene rings (Figure 4) in this arrangement. It is worth mentioning that a similar zigzag arrangement of biphenylene containing acene analogues proved to be beneficial for charge transfer and field effect mobilities as high as  $2.9 \text{ cm}^2 \text{ V}^{-1} \text{ s}^{-1}$  could be obtained by using this packing motif.<sup>[27]</sup> Additionally the electronic coupling is comparable to the reorganization energy (182 meV) discussed previously and therefore a bandlike transport, which should be highly efficient, is expected to take place.<sup>[16a]</sup> The coupling between molecules of adjacent columns along the crystallographic  $c$  axis (Figure 6a) is much smaller ( $t_{\text{h}}^{\text{b,dw}} = 28 \text{ meV}$ ). Therefore, hole transport in this structure is presumably highly anisotropic.

In the  $\delta_2$  modification coupling of the herringbone sheets along the crystallographic  $b$  axis determines the hole transport characteristics ( $t_{\text{h}}^{\text{b},\perp} = 27 \text{ meV}$ ). Moderate ( $t_{\text{h}}^{\text{c},\parallel} = 44 \text{ meV}$ ) to large transfer integrals ( $t_{\text{h}}^{\text{A,SS}} = 92 \text{ meV}$ ) exist between face-to-face stacked antiparallel dimers (Figure 7b and c) and edge-to-face stacked dimers with S...S interaction (Figure 7e), respectively. However, these dimers are isolated and therefore do not contribute to overall hole transfer.  $\pi$  stacking of unsubstituted triptycene wings (D, Figure 7d) are negligible.

For the crystal structure of **T-NTBT** a transfer integral between the dimer with the higher molecular overlap of  $t_{\text{h}}^{\text{A},\parallel} = 116 \text{ meV}$  was computed. For the dimer with the smaller molecular overlap the coupling is smaller ( $t_{\text{h}}^{\text{B},\parallel} = 71 \text{ meV}$ ) (Figure 8a and b). Both values are reasonably high, making this structure also interesting for efficient hole transport. As the holes have to pass through both dimers, the lower coupling is likely to limit the overall mobility.

## Conclusions

In summary, a three-step synthesis of a triptycene end-capped BTBT and its homologue NTBT, extended by one ring, was presented. Both compounds were soluble in common organic solvents and showed a high crystallization tendency. The relatively low molecular weight allowed sublimation, which is beneficial for both purification and device fabrication. DFT calculations further revealed that triptycene end-capping can also lower the reorganization energy through homoconjugation. By single-crystal X-ray diffraction five single-crystal structures of **T-BTBT** were obtained, two of them by sublimation methods. Antiparallel  $\pi$  dimers, comparable to those found for the previously published QPPs,<sup>[7a,b]</sup> were found in four of those structures. This once more illustrates the scope of the triptycene end-capping as a crystallographic synthon for enhanced cofacial  $\pi$  stacking. However, the overall packing was still herringbone-like. The polymorphism found for **T-BTBT** showed that the exact crystallization conditions also have significant impact on the molecular arrangement and thus have to be examined

closely to find favorable stacking motifs. One of the two polymorphs obtained by sublimation stacked in a rather unexpected herringbone-type arrangement with increased, cross-wise  $\pi$  stacking along the crystallographic  $a$  axis. **T-NTBT** crystallized in a brick-wall-like arrangement of two alternating  $\pi$  dimers. Out of these structures the latter two are especially promising for application in OFET devices. This was confirmed by calculated charge transfer integrals for hole transport. For **T-NTBT** high values of  $t_{\text{h}} = 71$ – $116 \text{ meV}$  along the  $\pi$  stacking axis were calculated. The exceptionally high transfer integral (177 meV) of **T-BTBT** together with a small reorganization energy and thus an expected bandlike hole transport makes this polymorph very promising for OFET application. Preliminary orienting tests on device fabrications with **T-BTBT** were less successful ( $1.4 \times 10^{-3} \text{ cm}^2 \text{ V}^{-1} \text{ s}^{-1}$ ). This might, among other reasons, also be related to the highly anisotropic character of carrier transport, which makes the relative orientation of the molecules to the electrodes a crucial factor. We are currently trying to optimize device parameters to improve the performance and to produce high performance OFET devices.

## Experimental Section

### General remarks

Bromo-2-phenylacetylene **4a** was prepared according to a literature known procedure.<sup>[28]</sup> All reagents and solvents were purchased from Fisher Scientific, Alfa Aesar, Sigma-Aldrich, TCI or VWR and were used without further purification unless otherwise noted. For thin-layer chromatography, silica gel 60 F254 plates from Merck were used and examined under UV irradiation ( $\lambda = 254$  and  $365 \text{ nm}$ ). Flash column chromatography was performed on silica gel from Sigma-Aldrich (particle size 0.04–0.063 mm) with petroleum ether (PE) and dichloromethane as the eluents. Melting points (not corrected) were measured by using a Büchi Melting Point B-545 instrument. IR spectra were recorded on a Ge ATR crystal by using a Bruker Lumos spectrometer. NMR spectra were recorded by using Bruker Avance DRX (300 MHz), Bruker Avance III (300 MHz), Bruker Avance III (400 MHz), and Bruker Avance III (500 MHz) spectrometers. Chemical shifts ( $\delta$ ) are reported in parts per million [ppm] relative to trace  $\text{CHCl}_3$  in the corresponding deuterated solvent. HRMS experiments were carried out by using a Fourier-Transform Ion Cyclotron Resonance (FT-ICR) mass spectrometer solariX (Bruker Daltonik, Bremen, Germany) equipped with a 7.0 T superconducting magnet and interfaced to an Apollo II Dual ESI/MALDI source. Absorption spectra were recorded on a Jasco UV-VIS V-730. Emission spectra were recorded on a Jasco FP-8300. Quantum yields were determined using an emission spectrometer equipped with an integration sphere (LabSphere®; diameter 6", coated with Spectrafect®). The system was calibrated with a primary light source.<sup>[29]</sup> The procedure from Würth et al.<sup>[30]</sup> was used with following settings for the emission spectrometer: bandwidth 3 nm, emission bandwidth 3 nm, integration time 1 s. Electrochemical data were obtained in a solution of TBAPF (tetra-*n*-butyl ammonium hexafluorophosphate) (0.05 M) in  $\text{CHCl}_3$  that contained 1 mM of the investigated compound, as indicated. Ferrocene (1 mM) was used as an internal standard. Cyclic voltammograms were obtained at a scan rate of  $0.05 \text{ V s}^{-1}$  with a Pt working electrode ( $0.78 \text{ mm}^2$ ), a Pt counter electrode, and an Ag reference electrode. Crystal structure analysis was accomplished by using a Bruker Apex-II diffractometer with a molybdenum source

( $\lambda(\text{Mo}_{\text{K}\alpha}) = 0.71073 \text{ \AA}$ ). Data were corrected for sample illumination, air and detector absorption, Lorentz, and polarization effects;<sup>[31]</sup> absorption by the crystal was treated numerically (Gaussian grid).<sup>[31,32]</sup> The structures were solved by using intrinsic phasing<sup>[33]</sup> or direct methods with dual-space recycling<sup>[34]</sup> and refined by using full-matrix least-squares methods on F2 against all unique reflections.<sup>[35]</sup> All non-hydrogen atoms were given anisotropic displacement parameters. Hydrogen atoms were input at calculated positions and refined with a riding model. When necessary, disordered groups and/or solvent molecules were subjected to suitable geometry and adp restraints and/or constraints.

Deposition Numbers 1987195, 1987196, 1987197, 1987198, 1987199, 1987200, 1987201, and 1987202 contain the supplementary crystallographic data for this paper. These data are provided free of charge by the joint Cambridge Crystallographic Data Centre and Fachinformationszentrum Karlsruhe Access Structures service.

## Synthetic procedures

**2-Bromo-3-iodotriptycene (3):** 1,4-Diiodo-2,5-dibromobenzene **1** (4.88 g, 10.0 mmol) and anthracene **2** (1.27 g, 7.14 mmol) were dissolved in abs. toluene (130 mL) under Ar-atmosphere and kept at room temperature with a water bath. 4.76 mL *n*BuLi (2.4 M solution in hexane, 11.4 mmol, 1.60 equiv.) was diluted with 2.4 mL abs. toluene and the resulting solution added dropwise over a period of 100 min. The reaction mixture was stirred for 15 h at room temperature, filtered through a pad of Celite® and the solvent was removed under reduced pressure to give 5.5 g of a dark yellow sticky solid. The crude product was recrystallized from acetone to remove the excess of anthracene by filtration. This procedure was repeated three times. The remaining solid was purified via column chromatography (SiO<sub>2</sub>, PE, [*R*<sub>f</sub> = 0.62, 0.43, 0.32, 0.24, **0.16**]) to obtain 2-bromo-3-iodotriptycene **3** as a colorless solid (537 mg, 16%). mp 215–220 °C. <sup>1</sup>H NMR (300 MHz, CDCl<sub>3</sub>):  $\delta$  [ppm] = 7.86 (s, 1H, *H*-1), 7.64 (s, 1H, *H*-4), 7.37 (dd, *J* = 5.3, 3.2 Hz, 4H, *H*-5/8), 7.02 (dd, *J* = 5.3, 3.2 Hz, 4H, *H*-6/7), 5.34 (s, 2H, *H*-9/10). <sup>13</sup>C NMR (50 MHz, CDCl<sub>3</sub>):  $\delta$  [ppm] = 147.6 (C-1a), 146.5 (C-4a), 144.3 (C-5a/8a), 144.2 (C-5a/8a), 135.0 (C-1), 127.9 (C-4), 125.83 (C-6/7), 125.79 (C-6/7), 125.76 (C-2/3), 124.01 (C-5/8), 123.98 (C-5/8), 96.6 (C-2/3), 53.4 (C-9/10), 53.0 (C-9/10). IR (ATR):  $\tilde{\nu}$  [cm<sup>-1</sup>] = 3068 (vw), 3041 (vw), 3023 (vw), 2968 (vw), 2923 (vw), 2852 (vw), 1944 (vw), 1904 (vw), 1786 (vw), 1751 (vw), 1737 (vw), 1588 (vw), 1552 (vw), 1479 (vw), 1457 (m), 1440 (m), 1363 (w), 1313 (vw), 1297 (vw), 1291 (vw), 1245 (vw), 1198 (vw), 1188 (w), 1170 (vw), 1161 (w), 1148 (vw), 1130 (vw), 1089 (w), 1026 (w), 933 (vw), 919 (m), 910 (w), 886 (m), 867 (w), 815 (w), 800 (w), 792 (w), 752 (s), 741 (vs.), 694 (vw), 654 (vw), 638 (w), 626 (m), 613 (w). HRMS (EI+): *m/z* = 457.9019 [M]<sup>+</sup> (calcd for [M]<sup>+</sup>: *m/z* = 457.9167), 377.9803 [M-Br]<sup>+</sup> (calcd for [M-Br]<sup>+</sup>: *m/z* = 378.9984), 329.9955 [M-I]<sup>+</sup> (calcd for [M-I]<sup>+</sup>: *m/z* = 331.0122). Elemental analysis calcd for C<sub>20</sub>H<sub>12</sub>BrI(C<sub>5</sub>H<sub>12</sub>)<sub>0.33</sub> [%]: C: 53.49, H: 3.17. Found: C: 53.26, H: 2.98.

**2-Bromo-3-[(2-bromophenyl)ethynyl]-triptycene (5a):** 2-Bromo-3-iodotriptycene **3** (205 mg, 0.45 mmol), alkyne **4a** (121 mg, 0.67 mmol), PdCl<sub>2</sub>(PPh<sub>3</sub>)<sub>2</sub> (16 mg, 0.02 mmol) and CuI (10 mg, 0.05 mmol) were dissolved in NEt<sub>3</sub> (2 mL) and stirred at room temperature for 14 h. The reaction mixture was poured onto water (10 mL) and extracted with ethyl acetate (2 × 20 mL). The combined organic layer was washed with 1 M HCl (2 × 20 mL) and dried over MgSO<sub>4</sub>. The solvent was removed under reduced pressure and the residue washed with acetone (3 mL) to give **5a** as a pale-yellow solid (192 mg, 83%). mp 225–229 °C. <sup>1</sup>H NMR (400 MHz, CDCl<sub>3</sub>):  $\delta$  [ppm] = 7.65 (s, 1H, *H*-1/10), 7.63 (s, 1H, *H*-1/10), 7.61 (dd, *J* = 8.1, 1.0 Hz, 1H, *H*-5/8), 7.57 (dd, *J* = 7.7, 1.6 Hz, 1H, *H*-5/8), 7.39 (dd, *J* =

5.2, 3.2 Hz, 4H, *H*-11/14), 7.29 (dt, *J* = 7.5, 1.3 Hz, 1H + CHCl<sub>3</sub>, *H*-6/7), 7.17 (dt, *J* = 7.8, 1.6 Hz, 1H, *H*-6/7), 7.03–7.01 (m, 4H, *H*-12/13), 5.42 (s, 1H, *H*-11/15), 5.40 (s, 1H, *H*-11/15). <sup>13</sup>C NMR (100 MHz, CDCl<sub>3</sub>):  $\delta$  [ppm] = 147.7 (C-1a/10a), 144.7 (C-1a/10a), 144.5 (C-14a/11a), 144.2 (C-14a/11a), 133.7 (C-5/8), 132.6 (C-5/8), 129.7 (C-6/7), 128.4 (C-1/10), 127.9 (C-1/10), 127.1 (C-6/7), 125.8 (C-4/9), 125.73 (C-12/13), 125.67 (C-12/13), 125.5 (C-4/9), 124.00 (C-11/14), 123.96 (C-11/14), 122.2 (C-2/3), 121.5 (C-2/3), 92.8 (C-3a/3b), 91.5 (C-3a/3b), 53.7 (C-15/16), 53.4 (C-15/16). HRMS (DART): *m/z* = 509.9617 [M]<sup>+</sup> (calcd for [M]<sup>+</sup>: *m/z* = 509.9619), 527.9960 [M+NH<sub>4</sub>]<sup>+</sup> (calcd for [M+NH<sub>4</sub>]<sup>+</sup>: *m/z* = 527.9957), 1020.9323 [2M+H]<sup>+</sup> (calcd for [2M+H]<sup>+</sup>: *m/z* = 1020.9310), 1037.9572 [2M+NH<sub>4</sub>]<sup>+</sup> (calcd for [2M+NH<sub>4</sub>]<sup>+</sup>: *m/z* = 1037.9576). IR (ATR):  $\tilde{\nu}$  [cm<sup>-1</sup>] = 3064 (vw), 3049 (vw), 3019 (w), 2954 (vw), 1940 (vw), 1904 (vw), 1793 (vw), 1584 (vw), 1556 (vw), 1486 (vw), 1473 (w), 1456 (m), 1452 (m), 1432 (w), 1421 (w), 1404 (vw), 1391 (w), 1321 (vw), 1293 (vw), 1256 (vw), 1191 (w), 1156 (w), 1143 (vw), 1114 (w), 1099 (vw), 1044 (w), 1026 (w), 974 (w), 946 (vw), 938 (vw), 932 (vw), 904 (vw), 891 (m), 872 (vw), 860 (w), 836 (w), 801 (w), 785 (vw), 744 (vs.), 708 (w), 678 (w), 654 (w), 643 (w), 626 (m). Elemental analysis calcd for C<sub>28</sub>H<sub>16</sub>Br<sub>2</sub>(H<sub>2</sub>O)<sub>0.5</sub> [%]: C: 64.52, H: 3.29. Found: C: 64.58, H: 3.72.

**Triptycenylothieno-[3,2-*b*][1]-benzothiophene (T-BTBT):** T-BTBT was synthesized according to a modified literature known procedure.<sup>[12]</sup> A suspension of 2-Bromo-3-[(2-bromophenyl)ethynyl]-triptycene **5a** (135 mg, 0.26 mmol), Na<sub>2</sub>S·H<sub>2</sub>O (60% purity, 137 mg, 1.05 mmol), CuI (10 mg, 0.05 mmol) and I<sub>2</sub> (134 mg, 0.53 mmol) were stirred under Ar-atmosphere in NMP (1.35 mL) for 24 h at 120 °C. After cooling to room temperature, the reaction mixture was quenched with water (8 mL), the precipitate collected by filtration and washed with water (20 mL). Purification via recrystallization from acetone gave triptycenylothieno-[3,2-*b*][1]-benzothiophene T-BTBT as a pale-yellow solid (57 mg, 51%). Further purification by sublimation (270 °C, 3 × 10<sup>-3</sup> mbar) gave pale yellow crystals. mp 313.6–314.0 °C (after sublimation). <sup>1</sup>H NMR: (400 MHz, CDCl<sub>3</sub>)  $\delta$  [ppm] = 7.90 (s, 1H, *H*-6) 7.89 (s, 1H, *H*-1), 7.89–7.87 (m, 2H, *H*-2), 7.84 (dd, *J* = 8.3 Hz, 2H, *H*-5), 7.45–7.41 (m, 5H, *H*-7/10/4), 7.36 (td, *J* = 7.7, 1.3 Hz, 1H, *H*-3), 7.03 (dd, *J* = 5.4, 3.1 Hz, 4H, *H*-8/9), 5.56 (s, 1H, *H*-11), 5.52 (s, 1H, *H*-12). <sup>13</sup>C NMR: (100 MHz, CDCl<sub>3</sub>)  $\delta$  [ppm] = 145.1 (C-6b/10a), 144.9 (C-5c), 143.0 (C-6a/10b), 142.9 (C-6a/10b), 142.1 (C-1c), 139.5 (C-5a), 133.5 (C-1b), 133.40 (C-6b/10a), 133.38 (C-1a), 130.4 (C-5b), 125.6 (C-8/9), 124.9 (C-3/4), 124.8 C-(7/10), 124.1 (C-2/5), 123.9 (C-7/10), 121.5 (C-2/5), 119.1 (C-6), 116.7 (C-1), 54.2 (C-11/12), 54.16 (C-11/12). HRMS (DART): *m/z* = 416.0710 [M]<sup>+</sup> (calcd for [M]<sup>+</sup>: *m/z* = 416.0693), 434.1049 [M+NH<sub>4</sub>]<sup>+</sup> (calcd for [M+NH<sub>4</sub>]<sup>+</sup>: *m/z* = 434.1032), 832.1455 [2M]<sup>+</sup> (calcd for [2M]<sup>+</sup>: *m/z* = 832.1387), 850.1764 [2M+NH<sub>4</sub>]<sup>+</sup> (calcd for [2M+NH<sub>4</sub>]<sup>+</sup>: *m/z* = 850.1725). IR (ATR):  $\tilde{\nu}$  [cm<sup>-1</sup>] = 1589 (vw), 1479 (vw), 1456 (m), 1433 (m), 1392 (vw), 1342 (vw), 1321 (w), 1313 (w), 1290 (w), 1252 (w), 1213 (w), 1182 (w), 1159 (w), 1126 (vw), 1099 (vw), 1038 (w), 1022 (w), 974 (vw), 933 (w), 920 (w), 876 (w), 864 (w), 850 (w), 825 (w), 802 (w), 764 (m), 746 (vs.), 737 (vs.), 723 (s), 706 (w), 683 (w), 665 (w), 644 (w), 627 (m), 602 (m), 557 (m), 540 (w), 515 (w), 494 (w), 478 (w), 467 (w), 453 (w), 430 (m), 407 (m). Elemental analysis calcd for C<sub>28</sub>H<sub>16</sub>S<sub>2</sub> [%]: C: 80.74, H: 3.87. Found: C: 80.68, H: 4.05. UV/Vis (CH<sub>2</sub>Cl<sub>2</sub>):  $\lambda_{\text{abs}}$  [nm] (lg  $\epsilon$ ) = 328 (4.49), 314 (4.53), 272 (4.31), 262 (4.33). Fluorescence (CH<sub>2</sub>Cl<sub>2</sub>):  $\lambda_{\text{em}}$  [nm] ( $\lambda_{\text{ex}}$  [nm]) = 340, 357, 373 (318). PLQY:  $\Phi$  [%] ( $\lambda_{\text{ex}}$  [nm], solvent) = 15 (314, CH<sub>2</sub>Cl<sub>2</sub>).

**2-Bromo-3-ethynynaphthalene (4b):** [(3-Bromonaphthalen-2-yl)ethynyl]-trimethylsilane<sup>[36]</sup> (120 mg, 0.39 mmol) was added to an ice cold solution of KOH (102 mg, 1.83 mmol) in MeOH (1 mL). After stirring 45 min. at room temperature the yellow suspension was diluted with CH<sub>2</sub>Cl<sub>2</sub> and washed with H<sub>2</sub>O (2 × 10 mL). The organic phases were combined, dried over MgSO<sub>4</sub> and the solvent



removed under reduced pressure. The yellow residue was purified by flash column chromatography (SiO<sub>2</sub>, PE [*R<sub>f</sub>* = 0.34, 0]) to give **4b** as a pale-yellow solid (76 mg, 85%). mp 98–99 °C (decomp.). <sup>1</sup>H NMR (400 MHz, CDCl<sub>3</sub>) δ [ppm] = 8.09 (s, 1H, *H*-1), 8.07 (s, 1H, *H*-4), 7.79–7.72 (m, 2H, *H*-5/8), 7.53–7.50 (m, 2H, *H*-6/7), 3.40 (s, 1H, *H*-3b). <sup>13</sup>C NMR (100 MHz, CDCl<sub>3</sub>) δ [ppm] = 134.4 (C-2/3), 134.1 (C-4a/8a), 131.7 (C-4a/8a), 131.2 (C-2/3), 128.0 (C-6/7), 127.8 (C-5/8), 127.1 (C-6/7), 127.0 (C-5/8), 121.7 (C-2/3), 121.6 (C-2/3), 82.3 (C-3a), 81.5 (C-3b). HRMS (EI+): *m/z* = 229.9699 [*M*]<sup>+</sup> (calcd for [*M*]<sup>+</sup>: *m/z* = 229.9731. IR (ATR):  $\tilde{\nu}$  [cm<sup>-1</sup>] = 3304 (w), 3287 (m), 3057 (vw), 2110 (vw), 1958 (vw), 1828 (vw), 1707 (vw), 1618 (vw), 1582 (w), 1487 (w), 1447 (w), 1423 (w), 1344 (vw), 1315 (w), 1269 (w), 1240 (w), 1207 (w), 1167 (vw), 1148 (w), 1130 (w), 1016 (vw), 988 (m), 957 (m), 891 (s), 822 (vw), 787 (vw), 752 (vs.), 685 (m), 675 (m), 656 (m), 611 (m). Elemental analysis calcd for C<sub>12</sub>H<sub>7</sub>Br [%]: C: 62.37, H: 3.05. Found: C: 62.77, H: 3.24.

**(9r,10r)-2-Bromo-3-[(3-bromonaphthalen-2-yl)ethynyl]-9,10-dihydro-9,10-[1,2]benzoanthracene (5b)**: To a suspension of 2-bromo-3-iodotriptycene **3** (79 mg, 0.17 mmol), CuI (3.3 mg, 17 μmol) and Pd(PPh<sub>3</sub>)<sub>2</sub>Cl<sub>2</sub> (6.1 mg, 8.7 μmol) in abs. THF (0.1 mL) and NEt<sub>3</sub> (0.35 mL) under Ar atmosphere a solution of 2-bromo-3-ethynyl naphthalene **4b** (48 mg, 0.21 mmol) in abs. THF (0.1 mL) was stirred. The dark suspension was added at room temperature for 14.5 h. H<sub>2</sub>O (15 mL) was added and the mixture extracted with CH<sub>2</sub>Cl<sub>2</sub> (3 × 10 mL). The combined organic phases were washed with 1 M HCl (2 × 10 mL) and dried over MgSO<sub>4</sub> to obtain a dark brown solid after removal of solvents. The residue was purified by flash column chromatography (CH<sub>2</sub>Cl<sub>2</sub>-PE = 1:10 [*R<sub>f</sub>* = 0.2, 0.08, 0] to 1:5) to give **5b** as a pale-yellow solid (81 mg, 84%). mp 255–262 °C. <sup>1</sup>H NMR (300 MHz, CDCl<sub>3</sub>) δ [ppm] = 8.10 (s, 1H, *H*-5/10), 8.09 (s, 1H, *H*-5/10), 7.76–7.71 (m, 2H, *H*-6/9), 7.66 (s, 1H, *H*-1/12), 7.65 (s, 1H, *H*-1/12), 7.51–7.48 (dd, *J* = 6.2, 3.2 Hz, 2H, *H*-7/8), 7.41–7.39 (m, 4H, *H*-13/16), 7.03 (dd, *J* = 3.2 Hz; 5.4 Hz, 4H, *H*-14/15), 5.43 (s, 1H, *H*-17/18), 5.40 (s, 1H, *H*-17/18). <sup>13</sup>C NMR (101 MHz, CDCl<sub>3</sub>) δ [ppm] = 147.7 (C-1a/12a), 144.7 (C-1a/12a), 144.5 (C-16a/13a), 144.2 (C-16a/13a), 133.9 (C-5a/9a), 133.5 (C-5/10), 131.9 (C-2/3), 131.2 (C-5/10), 128.5 (C-5a/9a), 127.9 (C-1/12), 127.8 (C-1/12), 127.78 (C-6/9), 127.0 (C-6/9), 125.8 (C-13/16), 125.7 (C-13/16), 124.0 (C-13/16), 123.97 (C-13/16), 122.7 (C-4/11), 122.2 (C-4/11), 121.9 (C-2/3), 121.6 (C-2/3), 92.5 (C-3a/3b), 91.8 (C-3a/3b), 53.7 (C-17/18), 53.4 (C-17/18). HRMS (EI+): *m/z* = 559.9598 [*M*]<sup>+</sup> (calcd for [*M*]<sup>+</sup>: *m/z* = 559.9775. IR (ATR):  $\tilde{\nu}$  [cm<sup>-1</sup>] = 3059 (vw), 2957 (vw), 2208 (vw), 1944 (vw), 1906 (vw), 1794 (vw), 1585 (vw), 1491 (w), 1458 (m), 1447 (w), 1425 (w), 1391 (w), 1327 (vw), 1294 (vw), 1261 (vw), 1196 (w), 1159 (vw), 1144 (w), 1115 (w), 1022 (vw), 1003 (vw), 961 (w), 891 (m), 883 (m), 858 (w), 849 (vw), 822 (vw), 800 (w), 787 (vw), 748 (vs.), 743 (vs.), 708 (w), 671 (vw), 658 (w), 642 (w), 625 (m), 613 (vw). Elemental analysis calcd for C<sub>32</sub>H<sub>18</sub>Br<sub>2</sub>·H<sub>2</sub>O [%]: C: 66.23, H: 3.47. Found: C: 65.89, H: 3.48.

**(8r,13r)-8,13-dihydro-8,13-[1,2]benzoanthra[2,3-b]naphtho[2',3':4,5]thieno[2,3-d]thiophene (T-NTBT)**: T-NTBT was synthesized according to a modified literature known procedure.<sup>[12]</sup> A suspension of 2-bromo-3-[(3-bromonaphthalen-2-yl)ethynyl]-tritycene **5b** (225 mg, 0.40 mmol), Na<sub>2</sub>S·H<sub>2</sub>O (60% purity, 208 mg, 1.60 mmol), CuI (15 mg, 0.08 mmol) and I<sub>2</sub> (203 mg, 0.80 mmol) were stirred under Ar atmosphere in NMP (2 mL) for 24 h at 120 °C. After cooling to room temperature, the mixture was quenched with water (30 mL), filtered and washed with distilled water (20 mL), MeOH (20 mL) and petroleum ether (10 mL). After column chromatography (PE:CHCl<sub>3</sub> = 3:1 [*R<sub>f</sub>* = 0.33, 0]) the crude product was recrystallized from PE/CHCl<sub>3</sub> to give naphthothienotriptycenyleno-benzothiophene T-NTBT as a pale yellow solid (11 mg, 24 μmol, 6%). mp > 410 °C. <sup>1</sup>H NMR (300 MHz, CDCl<sub>3</sub>) δ [ppm] =

8.34 (s, 1H, *H*-2), 8.27 (s, 1H, *H*-7), 7.98 (dd, *J* = 6.2, 3.5 Hz, 1H, *H*-6), 7.93 (s, 1H, *H*-8), 7.90 (dd, *J* = 5.7, 2.9 Hz, 1H, *H*-3), 7.89 (s, 1H, *H*-1), 7.49 (dd, *J* = 6.4, 3.2 Hz, 2H, *H*-4/5), 7.45–7.42 (m, 4H, *H*-9/12), 7.03 (dd, *J* = 3.2 Hz; 5.3 Hz, 4H, *H*-10/11), 5.57 (s, 1H, *H*-13), 5.54 (s, 1H, *H*-14). <sup>13</sup>C NMR: (100 MHz, CDCl<sub>3</sub>) δ [ppm] = 145.1 (C-8b/12a), 144.8 (C-8b/12a), 143.3 (C-12b), 143.1 (C-8a), 140.7 (C-1c), 140.0 (C-7a), 134.4 (C-1a), 132.7 (C-1b/7c), 132.5 (C-1b/7c), 131.32 (C-2a/6a), 131.27 (C-2a/6a), 130.5 (C-7b), 128.3 (C-3/6), 127.4 (C-3/6), 125.8 (C-10/11/4/5), 125.75 (C-10/11/4/5), 125.68 (C-4/5/10/11), 125.66 (C-10/11/4/5), 123.9 (C-9/12), 122.5 (C-2/7), 119.5 (C-2/7), 119.1 (C-8), 117.0 (C-1), 54.24 (C-13/14), 54.16 (C-13/14). HRMS (DART): *m/z* = 466.0831 [*M*]<sup>+</sup> (calcd for [*M*]<sup>+</sup>: *m/z* = 466.0850), 932.1664 [2*M*]<sup>+</sup> (calcd for [2*M*]<sup>+</sup>: *m/z* = 932.1700), 950.2004 [2*M*+NH<sub>4</sub>]<sup>+</sup> (calcd for [2*M*+NH<sub>4</sub>]<sup>+</sup>: *m/z* = 950.2038), 1398.2442 [3*M*]<sup>+</sup> (calcd for [3*M*]<sup>+</sup>: *m/z* = 1398.2550). IR (ATR):  $\tilde{\nu}$  [cm<sup>-1</sup>] = 3063 (vw), 3017 (vw), 2922 (w), 2853 (w), 1597 (vw), 1456 (m), 1425 (w), 1377 (w), 1335 (vw), 1310 (w), 1281 (w), 1186 (w), 1153 (w), 1132 (vw), 1124 (vw), 1022 (w), 949 (vw), 878 (m), 862 (m), 816 (w), 783 (vw), 737 (vs.), 702 (w), 689 (w), 644 (vw), 627 (m), 613 (w). Elemental analysis calcd for C<sub>32</sub>H<sub>18</sub>S<sub>2</sub>(CH<sub>2</sub>Cl<sub>2</sub>)<sub>0.2</sub> [%]: C: 79.97, H: 3.84. Found: C: 80.09, H: 4.10. UV/Vis (CH<sub>2</sub>Cl<sub>2</sub>): λ<sub>abs</sub> [nm] (lg ε) = 375 (4.20), 356 (4.26), 329 (4.33), 316 (4.19), 299 (4.85), 287 (4.60), 255 (4.54). Fluorescence (CH<sub>2</sub>Cl<sub>2</sub>): λ<sub>em</sub> [nm] (λ<sub>ex</sub> [nm]) = 388, 406, 428<sup>sh</sup> (365). PLQY: Φ [%] (λ<sub>ex</sub> [nm], solvent) = 18 (330, CH<sub>2</sub>Cl<sub>2</sub>).

## Acknowledgements

The authors are grateful to “Deutsche Forschungsgemeinschaft” supporting this project (within the collaborative research center SFB1249 “N-heteropolycyclic compounds as functional materials” (TP-A04, TP-B02 and TP-C06). We would like to thank Till Kahlstorf for preliminary research. Open access funding enabled and organized by Projekt DEAL.

## Conflict of interest

The authors declare no conflict of interest.

**Keywords:** benzothienobenzothiophene · charge transfer · crystal engineering · triptycene

- [1] a) C.-T. Hsieh, C.-Y. Chen, H.-Y. Lin, C.-J. Yang, T.-J. Chen, K.-Y. Wu, C.-L. Wang, *J. Phys. Chem. C* **2018**, *122*, 16242–16248; b) Y. Diao, K. M. Lenn, W.-Y. Lee, M. A. Blood-Forsythe, J. Xu, Y. Mao, Y. Kim, J. A. Reinspach, S. Park, A. Aspuru-Guzik, G. Xue, P. Clancy, Z. Bao, S. C. B. Mannsfeld, *J. Am. Chem. Soc.* **2014**, *136*, 17046–17057; c) A. F. Paterson, S. Singh, K. J. Fallon, T. Hodsdon, Y. Han, B. C. Schroeder, H. Bronstein, M. Heeney, I. McCulloch, T. D. Anthopoulos, *Adv. Mater.* **2018**, *30*, 1801079.
- [2] a) T. Steiner, *Angew. Chem. Int. Ed.* **2002**, *41*, 48–76; b) T. Steiner, *Angew. Chem.* **2002**, *114*, 50–80.
- [3] a) P. Metrangolo, G. Resnati, *Chem. Eur. J.* **2001**, *7*, 2511–2519; b) G. R. Desiraju, R. Parthasarathy, *J. Am. Chem. Soc.* **1989**, *111*, 8725–8726.
- [4] a) C. A. Hunter, J. K. M. Sanders, *J. Am. Chem. Soc.* **1990**, *112*, 5525–5534; b) C. R. Martinez, B. L. Iverson, *Chem. Sci.* **2012**, *3*, 2191–2201; c) C. Janiak, *J. Chem. Soc. Dalton Trans.* **2000**, 3885–3896.
- [5] a) J. L. Brédas, J. P. Calbert, D. A. da Silva Filho, J. Cornil, *Proc. Natl. Acad. Sci. USA* **2002**, *99*, 5804–5809; b) C. Reese, Z. Bao, *J. Mater. Chem.* **2006**, *16*, 329–333.
- [6] a) B. Kohl, F. Rominger, M. Mastalerz, *Org. Lett.* **2014**, *16*, 704–707; b) B. Kohl, F. Rominger, M. Mastalerz, *Angew. Chem. Int. Ed.* **2015**, *54*, 6051–6056; *Angew. Chem.* **2015**, *127*, 6149–6154; c) B. Kohl, M. V. Bohnwagner, F. Rominger, H. Wadepohl, A. Dreuw, M. Mastalerz, *Chem. Eur. J.*

- 2016, 22, 646–655; d) D. Reinhard, F. Rominger, M. Mastalerz, *J. Org. Chem.* **2015**, 80, 9342–9348; e) K. Baumgärtner, A. L. Meza Chinchá, A. Dreuw, F. Rominger, M. Mastalerz, *Angew. Chem. Int. Ed.* **2016**, 55, 15594–15598; *Angew. Chem.* **2016**, 128, 15823–15827; f) K. Baumgärtner, F. Rominger, M. Mastalerz, *Chem. Eur. J.* **2018**, 24, 8751–8755; g) B. Kohl, K. Baumgärtner, F. Rominger, M. Mastalerz, *Eur. J. Org. Chem.* **2019**, 4891–4896.
- [7] a) L. Ueberricke, D. Holub, J. Kranz, F. Rominger, M. Elstner, M. Mastalerz, *Chem. Eur. J.* **2019**, 25, 11121–11134; b) L. Ueberricke, S. Wieland, F. Rominger, M. Mastalerz, *Organic Materials* **2019**, 01, 50–62; c) E. Prantl, B. Kohl, D. Rylvlin, P. Biegger, H. Wadepohl, F. Rominger, U. H. F. Bunz, M. Mastalerz, S. R. Waldvogel, *ChemPlusChem* **2019**, 84, 1239–1244.
- [8] a) K. Takimiya, H. Ebata, K. Sakamoto, T. Izawa, T. Otsubo, Y. Kunugi, *J. Am. Chem. Soc.* **2006**, 128, 12604–12605; b) H. Ebata, T. Izawa, E. Miyazaki, K. Takimiya, M. Ikeda, H. Kuwabara, T. Yui, *J. Am. Chem. Soc.* **2007**, 129, 15732–15733; c) C. Niebel, Y. Kim, C. Ruzié, J. Karpinska, B. Chattopadhyay, G. Schweicher, A. Richard, V. Lemaure, Y. Olivier, J. Cornil, A. R. Kennedy, Y. Diao, W.-Y. Lee, S. Mannsfeld, Z. Bao, Y. H. Geerts, *J. Mater. Chem. C* **2015**, 3, 674–685; d) C. Ruzié, J. Karpinska, A. R. Kennedy, Y. H. Geerts, *J. Org. Chem.* **2013**, 78, 7741–7748; e) T. Yamamoto, T. Nishimura, T. Mori, E. Miyazaki, I. Osaka, K. Takimiya, *Org. Lett.* **2012**, 14, 4914–4917; f) T. Yamamoto, K. Takimiya, *J. Am. Chem. Soc.* **2007**, 129, 2224–2225; g) T. Mori, T. Nishimura, T. Yamamoto, I. Doi, E. Miyazaki, I. Osaka, K. Takimiya, *J. Am. Chem. Soc.* **2013**, 135, 13900–13913; h) K. Niimi, S. Shinamura, I. Osaka, E. Miyazaki, K. Takimiya, *J. Am. Chem. Soc.* **2011**, 133, 8732–8739.
- [9] a) K. Takimiya, S. Shinamura, I. Osaka, E. Miyazaki, *Adv. Mater.* **2011**, 23, 4347–4370; b) K. Takimiya, T. Yamamoto, H. Ebata, T. Izawa, *Sci. Technol. Adv. Mater.* **2007**, 8, 273–276.
- [10] Y. Yuan, G. Giri, A. L. Ayzner, A. P. Zoombelt, S. C. B. Mannsfeld, J. Chen, D. Nordlund, M. F. Toney, J. Huang, Z. Bao, *Nature Commun.* **2014**, 5, 3005.
- [11] S. Haas, Y. Takahashi, K. Takimiya, T. Hasegawa, *Appl. Phys. Lett.* **2009**, 95, 022111.
- [12] Y. Li, C. Nie, H. Wang, X. Li, F. Verpoort, C. Duan, *Eur. J. Org. Chem.* **2011**, 7331–7338.
- [13] R. Rieger, K. Müllen, *J. Phys. Org. Chem.* **2010**, 23, 315–325.
- [14] T. Yamamoto, S. Shinamura, E. Miyazaki, K. Takimiya, *Bull. Chem. Soc. Jpn.* **2010**, 83, 120–130.
- [15] K. Sakanoue, M. Motoda, M. Sugimoto, S. Sakaki, *J. Phys. Chem. A* **1999**, 103, 5551–5556.
- [16] a) E.-G. Kim, V. Coropceanu, N. E. Gruhn, R. S. Sánchez-Carrera, R. Snoberger, A. J. Matzger, J.-L. Brédas, *J. Am. Chem. Soc.* **2007**, 129, 13072–13081; b) R. S. Sánchez-Carrera, S. Atahan, J. Schrier, A. Aspuru-Guzik, *J. Phys. Chem. C* **2010**, 114, 2334–2340.
- [17] a) J.-L. Brédas, D. Beljonne, V. Coropceanu, J. Cornil, *Chem. Rev.* **2004**, 104, 4971–5004; b) V. Coropceanu, J. Cornil, D. A. da Silva Filho, Y. Olivier, R. Silbey, J.-L. Brédas, *Chem. Rev.* **2007**, 107, 926–952.
- [18] D. A. da Silva Filho, E.-G. Kim, J.-L. Brédas, *Adv. Mater.* **2005**, 17, 1072–1076.
- [19] V. Coropceanu, O. Kwon, B. Wex, B. R. Kaafarani, N. E. Gruhn, J. C. Durivage, D. C. Neckers, J.-L. Brédas, *Chem. Eur. J.* **2006**, 12, 2073–2080.
- [20] a) T. Doerner, R. Gleiter, T. A. Robbins, P. Chayangkoon, D. A. Lightner, *J. Am. Chem. Soc.* **1992**, 114, 3235–3241; b) K. Kawasumi, T. Wu, T. Zhu, H. S. Chae, T. Van Voorhis, M. A. Baldo, T. M. Swager, *J. Am. Chem. Soc.* **2015**, 137, 11908–11911; c) M. R. Talipov, T. S. Navale, R. Rathore, *Angew. Chem. Int. Ed.* **2015**, 54, 14468–14472; *Angew. Chem.* **2015**, 127, 14676–14680.
- [21] I. S. Antonijević, G. V. Janjić, M. K. Milčić, S. D. Zarić, *Cryst. Growth Des.* **2016**, 16, 632–639.
- [22] a) R. G. Kepler, *Phys. Rev.* **1960**, 119, 1226–1229; b) Y. Maruyama, H. Inokuchi, *Bull. Chem. Soc. Jpn.* **1967**, 40, 2073–2077.
- [23] a) M. Elstner, D. Porezag, G. Jungnickel, J. Elsner, M. Haugk, T. Frauenheim, S. Suhai, G. Seifert, *Phys. Rev. B* **1998**, 58, 7260–7268; b) A. Kubas, F. Hoffmann, A. Heck, H. Oberhofer, M. Elstner, J. Blumberger, *J. Chem. Phys.* **2014**, 140, 104105; c) A. Kubas, F. Gajdos, A. Heck, H. Oberhofer, M. Elstner, J. Blumberger, *Phys. Chem. Chem. Phys.* **2015**, 17, 14342–14354; d) A. Heck, J. J. Kranz, T. Kubař, M. Elstner, *J. Chem. Theory Comput.* **2015**, 11, 5068–5082; e) A. Heck, J. J. Kranz, M. Elstner, *J. Chem. Theory Comput.* **2016**, 12, 3087–3096; f) T. Kubař, M. Elstner, *J. Royal Soc. Interface* **2013**, 10, 20130415; g) T. Kubař, M. Elstner, *J. Phys. Chem. B* **2010**, 114, 11221–11240; h) G. Lüdemann, I. A. Solov'ov, T. Kubař, M. Elstner, *J. Am. Chem. Soc.* **2015**, 137, 1147–1156; i) G. Lüdemann, P. B. Woiczikowski, T. Kubař, M. Elstner, T. B. Steinbrecher, *J. Phys. Chem. B* **2013**, 117, 10769–10778; j) D. Holub, H. Ma, N. Krauß, T. Lamparter, M. Elstner, N. Gillet, *Chem. Sci.* **2018**, 9, 1259–1272; k) B. Aradi, B. Hourahine, T. Frauenheim, *J. Phys. Chem. A* **2007**, 111, 5678–5684.
- [24] F. Valiyev, W.-S. Hu, H.-Y. Chen, M.-Y. Kuo, I. Chao, Y.-T. Tao, *Chem. Mater.* **2007**, 19, 3018–3026.
- [25] M. Watanabe, Y. J. Chang, S.-W. Liu, T.-H. Chao, K. Goto, M. M. Islam, C.-H. Yuan, Y.-T. Tao, T. Shinmyozu, T. J. Chow, *Nat. Chem.* **2012**, 4, 574.
- [26] K. A. McGarry, W. Xie, C. Sutton, C. Risko, Y. Wu, V. G. Young, J.-L. Brédas, C. D. Frisbie, C. J. Douglas, *Chem. Mater.* **2013**, 25, 2254–2263.
- [27] J. Wang, M. Chu, J.-X. Fan, T.-K. Lau, A.-M. Ren, X. Lu, Q. Miao, *J. Am. Chem. Soc.* **2019**, 141, 3589–3596.
- [28] R. Diercks, K. P. C. Vollhardt, *Angew. Chem. Int. Ed. Engl.* **1986**, 25, 266–268; *Angew. Chem.* **1986**, 98, 268–270.
- [29] P. C. DeRose, E. A. Early, G. W. Kramer, *Rev. Sci. Instrum.* **2007**, 78, 033107.
- [30] C. Würth, M. Grabolle, J. Pauli, M. Spieles, U. Resch-Genger, *Nat. Protoc.* **2013**, 8, 1535.
- [31] CrysAlisPro, Agilent Technologies, Oxford (UK) **2011–2014**.
- [32] W. R. Busing, H. A. Levy, *Acta Crystallogr.* **1957**, 10, 180–182.
- [33] a) G. M. Sheldrick, SHELXT, University of Göttingen and Bruker AXS GmbH, Karlsruhe (Germany), **2012–2014**; b) M. Ruf, B. C. Noll, Application Note SC-XRD 503, Bruker AXS GmbH, Karlsruhe (Germany), **2014**; c) G. Sheldrick, *Acta Crystallogr. Sect. A* **2015**, 71, 3–8.
- [34] M. C. Burla, R. Caliandro, M. Camalli, B. Carrozzini, G. L. Cascarano, L. De Caro, C. Giacovazzo, G. Polidori, D. Siliqi, R. Spagna, *J. Appl. Crystallogr.* **2007**, 40, 609–613.
- [35] a) G. M. Sheldrick, SHELXL-20xx, University of Göttingen and Bruker AXS GmbH, Karlsruhe (Germany) **2012–2014**; b) G. Sheldrick, *Acta Crystallogr. Sect. A* **2008**, 64, 112–122.
- [36] a) H. Hart, A. Bashir-Hashemi, J. Luo, M. A. Meador, *Tetrahedron* **1986**, 42, 1641–1654; b) M. Klein, B. König, *Tetrahedron* **2004**, 60, 1087–1092.

Manuscript received: March 4, 2020

Revised manuscript received: April 28, 2020

Accepted manuscript online: May 5, 2020

Version of record online: September 11, 2020